Cell, Vol. 120, 85–98, January 14, 2005, Copyright ©2005 by Elsevier Inc. DOI 10.1016/j.cell.2004.11.048

Subtype-Specific and ER Lumenal Environment-Dependent Regulation of Inositol 1,4,5-Trisphosphate Receptor Type 1 by ERp44

Takayasu Higo,[1,2] Mitsuharu Hattori,[1,3,6] Takeshi Nakamura,[4] Tohru Natsume,[5] Takayuki Michikawa,[1] and Katsuhiko Mikoshiba[1,2,4,*]

[1]Department of Molecular Neurobiology
Institute of Medical Science
University of Tokyo
4-6-1 Shirokanedai, Minato-ku
Tokyo 108-8639
Japan

[2]Laboratory for Developmental Neurobiology
Brain Science Institute
RIKEN, Wako, Saitama 351-0198
Japan

[3]PRESTO

[4]Calcium Oscillation Project
ICORP, JST
Kawaguchi, Saitama 332-0012
Japan

[5]Protein Network Team
Functional Genome Group
Japan Biological Information Research Center
Koto-ku
Tokyo 135-8073
Japan

Summary

Inositol 1,4,5-trisphosphate receptors (IP_3Rs) are intracellular channel proteins that mediate Ca^{2+} release from the endoplasmic reticulum (ER) and are involved in many biological processes and diseases. IP_3Rs are differentially regulated by a variety of cytosolic proteins, but their regulation by ER lumenal protein(s) remains largely unexplored. In this study, we found that ERp44, an ER lumenal protein of the thioredoxin family, directly interacts with the third lumenal loop of IP_3R type 1 (IP_3R1) and that the interaction is dependent on pH, Ca^{2+} concentration, and redox state: the presence of free cysteine residues in the loop is required. Ca^{2+}-imaging experiments and single-channel recording of IP_3R1 activity with a planar lipid bilayer system demonstrated that IP_3R1 is directly inhibited by ERp44. Thus, ERp44 senses the environment in the ER lumen and modulates IP_3R1 activity accordingly, which should in turn contribute to regulating both intralumenal conditions and the complex patterns of cytosolic Ca^{2+} concentrations.

Introduction

The cytosolic Ca^{2+} concentration ($[Ca^{2+}]_C$) is the focal point of many signal transduction pathways and regulates a variety of cellular activities ranging from fertilization to cell death (Berridge et al., 2003). $[Ca^{2+}]_C$ is tightly regulated in terms of time, space, and amplitude, and cells extract specific information based on these parameters. Ca^{2+} ions can be supplied to the cytosol from the extracellular space or from intracellular Ca^{2+} stores, such as the endoplasmic reticulum (ER). Dysfunction of molecules involved in $[Ca^{2+}]_C$ regulation is assumed to play a major role in apoptosis (Orrenius et al., 2003) and neuropathological conditions, including Huntington's and Alzheimer's diseases (Paschen, 2003; Mattson, 2004). Inositol 1,4,5-trisphosphate receptors (IP_3Rs) are Ca^{2+} release channels on the ER that play a critical role in the generation of complex $[Ca^{2+}]_C$ patterning, e.g., Ca^{2+} waves and oscillations (Patterson et al., 2004). There are three IP_3R subtypes in birds and mammals, IP_3R1, IP_3R2, and IP_3R3, and they share basic properties but differ in terms of regulation and distribution (Taylor et al., 1999; Patterson et al., 2004). IP_3R1 is the dominant subtype in the brain (Taylor et al., 1999) and has been implicated in neuronal development (Takei et al., 1998; Xiang et al., 2002), in higher functions of the central nervous system (Inoue et al., 1998; Nishiyama et al., 2000), and in human neuropathology (Tang et al., 2003). A striking feature of IP_3Rs is the presence of very large cytosolic regions, including the IP_3 binding core (Patterson et al., 2004). The channel domain contains six transmembrane domains, and as a result there are three "loops" that reside in the ER lumen (Figure 1A). The third lumenal loop (L3) is the largest and can be divided into two subdomains. The first half, the L3V domain, has highly divergent primary sequences according to the subtype (Figure 1B), while the second half, the L3C domain, which includes the pore-forming region (Patterson et al., 2004), is almost completely conserved among types and species. Interestingly, the primary sequence of the L3V domain of each IP_3R subtype is well conserved among animal species, suggesting that this domain is involved in subtype-specific regulation. However, the function of the L3V domain remains largely unexplored.

It is evident that the intralumenal environment of the ER regulates the function of numerous proteins (Berridge et al., 2003), but how it regulates IP_3R activity remains unclear despite a great deal of research. For example, whether IP_3R is directly regulated by the Ca^{2+} concentration in the ER lumen ($[Ca^{2+}]_{ER}$) is still a matter of debate (Caroppo et al., 2003 and references therein). Calreticulin (CRT), an ER lumenal lectin with high Ca^{2+} binding capacity, regulates IP_3-induced Ca^{2+} release (IICR) (Camacho and Lechleiter, 1995; Roderick et al., 1998), but whether or not this is a direct effect on IP_3R remains unknown because CRT critically regulates the activity of sarcoendoplasmic reticulum Ca^{2+} ATPase (SERCA) 2b (Li and Camacho, 2004). Chromogranins that mainly reside in secretory granules associate with the L3C domain of IP_3Rs and modulate the activities of IP_3Rs (Thrower et al., 2003; Choe et al., 2004). However, the mechanisms by which interactions between chromogranins and IP_3Rs are regulated, and their physiological significance, remain unknown.

*Correspondence: mikosiba@ims.u-tokyo.ac.jp
[6]Present address: Department of Biomedical Science, Graduate School of Pharmaceutical Sciences, Nagoya City University, Mizuho-ku, Nagoya, Aichi 467-8603, Japan.

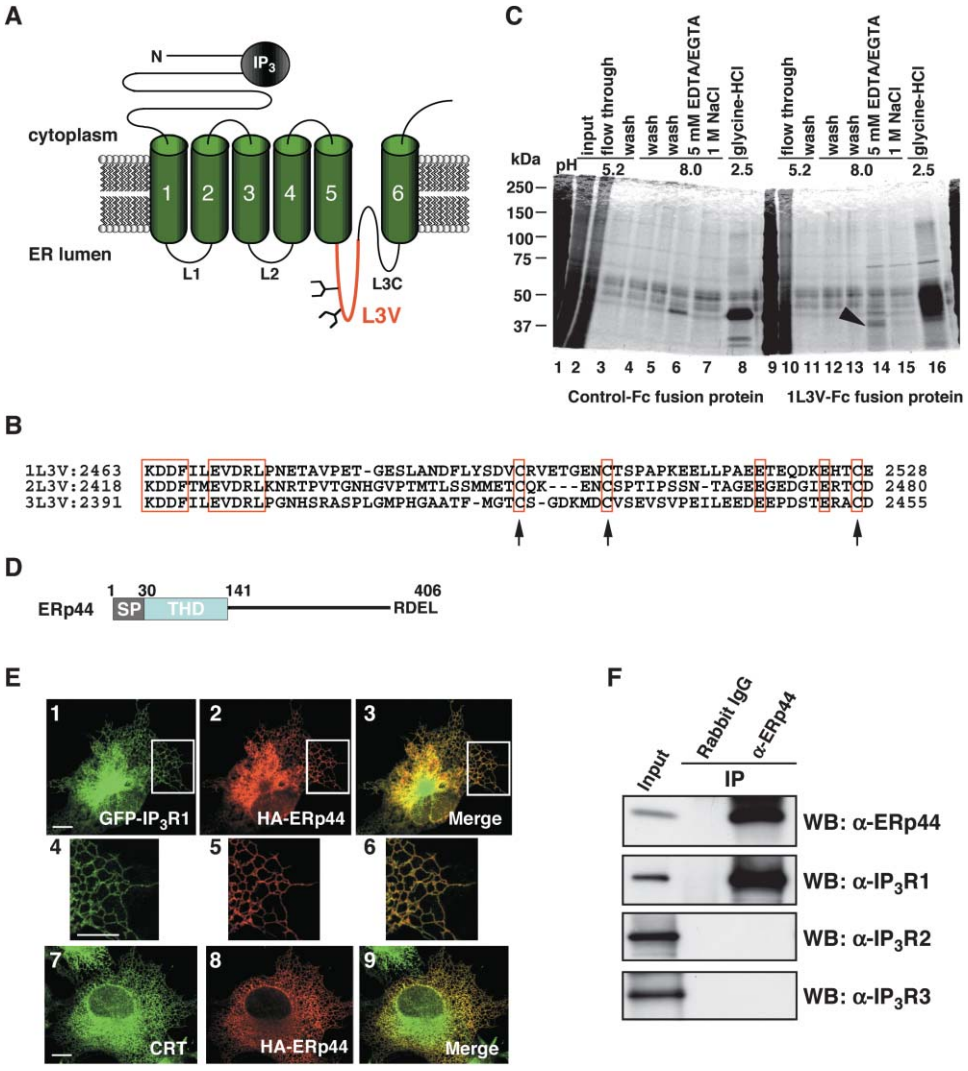

Figure 1. Identification of ERp44 as a Protein Binding to the L3V Domain of IP_3R1

(A) Schematic representation of the structure of IP_3Rs. IP_3Rs contain six membrane-spanning regions (green) and three lumenal domains, L1, L2, and L3. L3 is divided into L3V (red) and L3C. IP_3 binds to the N-terminal cytosolic region. L3V contains two glycosylation sites.

(B) Sequence comparison of the L3V of three subtypes of mouse IP_3R. Conserved amino acid residues are shown (red box). Conserved cysteine residues are indicated by arrows.

(C) Purification of 1L3V-interacting proteins. Mouse cerebellar microsomal fractions solubilized in acidic solution (pH 5.2) were added to either a control-Fc or a 1L3V-Fc column. The columns were washed with the same buffer (lanes 3 and 11), neutral buffer (lanes 4 and 5 and 12 and 13), and finally eluted with neutral buffer containing EGTA/EDTA (lanes 6 and 14), with buffer containing 1M NaCl (lanes 7 and 15), and with glycine-HCl solution (lanes 8 and 16). The arrowhead indicates the 45 kDa band that specifically binds to 1L3V-Fc, and it turned out to be ERp44.

(D) Structure of ERp44. The signal peptide (SP, aa 1–30), thioredoxin homology domain (THD, aa 31–141), and ER retention signal RDEL motif are shown.

(E) ERp44 colocalizes with IP_3R1 in the ER. COS-7 cells expressing HA-ERp44 and GFP-IP_3R1 were stained with α-HA (panels 1–3). The boxed regions in panels 1–3 are shown at increased magnification in panels 4–6, respectively. The cells expressing HA-ERp44 were stained with α-CRT and α-HA (panels 7–9). Scale bar, 10 μm.

(F) In vivo interaction between ERp44 and IP_3R1. HeLa cells were treated with a membrane-permeable crosslinker, DSP, and then solubilized. The cell lysates were subjected to IP with control rabbit IgG or α-ERp44. The lysate (Input) and IP samples were analyzed by Western blotting (WB) with indicated antibodies.

To elucidate the molecular mechanism underlying subtype-specific regulation of IP_3Rs on the ER lumen side, we searched for proteins that bind to the L3V domain of IP_3Rs. We succeeded in identifying ERp44, a thioredoxin (TRX) family protein previously implicated in oxidative protein folding, as a protein that specifically binds to the L3V domain of IP_3R1. Herein, we present strong evidence that ERp44 directly inhibits the channel activity of the IP_3R1 in a pH-, redox state-, and $[Ca^{2+}]_{ER}$-dependent manner. This is the first demonstration of negative regulation of IP_3Rs by a specific binding protein in the ER lumen. We anticipate that our results will contribute to understanding of the mechanism by which cells integrate various signals from the extracellular mi-

lieu and from the ER lumen in generating complex Ca^{2+} signaling patterns.

Results

Identification of ERp44 as a Binding Protein of the L3V Domain of IP_3R1

Our first goal was to identify proteins that bind to the L3V domain of IP_3Rs. Yeast two-hybrid screening was considered inappropriate as a method because the chemical conditions in the nucleus are completely different from those in the ER lumen. We therefore produced 1L3V-Fc protein by fusing the secretion signal and human immunoglobulin Fc domain to the N and C termini, respectively, of the L3V domain of IP_3R1 (1L3V) and then used it to prepare affinity resin. When an initial attempt under neutral conditions (pH 7.5, data not shown) failed to detect any specific 1L3V-Fc binding protein in the mouse cerebellar microsomal fraction, we performed a similar experiment under acidic conditions (pH 5.2) and succeeded in identifying two proteins that bound specifically to 1L3V-Fc (Figure 1C). Analysis of the bands by matrix-assisted laser desorption/ionization-time of flight mass spectrometry revealed the 44 kDa protein to be ERp44 (Anelli et al., 2002). The 85 kDa protein was identified as aconitase, a mitochondrial protein, and was not further characterized in this study. We then searched for binding proteins for the L3 domains of IP_3R2 and IP_3R3 (2L3V or 3L3V, respectively) in mouse brain, employing the same procedures, but detected none (data not shown).

ERp44 is an ER lumenal protein of the TRX family and contains a signal peptide, TRX-homology domain (THD), and an ER retention signal, RDEL (Figure 1D). ERp44 is widely expressed in mouse tissues (Supplemental Figure S1 at http://www.cell.com/cgi/content/full/120/1/85/DC1/). Hemagglutinin A epitope (HA)-tagged ERp44 (Anelli et al., 2002), alone or with GFP-IP_3R1, was expressed in COS-7 cells (Figure 1E). HA-ERp44 was observed as a diffuse network with GFP-IP_3R1 and endogenous CRT (Figure 1E), indicating that ERp44 colocalizes with IP_3R1 in the ER.

To confirm the interaction between IP_3R1 and ERp44, we raised polyclonal antibody against ERp44 and conducted immunoprecipitation (IP) experiments. Both IP_3R1 and ERp44 were, however, severely degraded when whole-cell lysates were prepared with acidic buffer (in which an association had been observed in the experiments shown in Figure 1C), presumably by lysosomal proteases (data not shown). To circumvent this, HeLa cells were first treated with a membrane-permeable crosslinker, dithiobis[succinimidylpropionate] (DSP), and IP was performed in neutral buffer. Under these conditions, anti-ERp44 antibody coprecipitated IP_3R1, but not IP_3R2 or IP_3R3 (Figure 1F), indicating that endogenous ERp44 and IP_3R1 exist in the same complex in vivo.

ERp44 Specifically Interacts with IP_3R1, but Not with IP_3R2 or IP_3R3, in a Condition-Dependent Manner

To further characterize the association between ERp44 and IP_3Rs, we performed a series of pulldown experiments with recombinant proteins. Glutathione (GSH) *S*-transferase (GST) and maltose binding protein (MBP) were fused to 1L3V and ERp44, respectively (Figure 2A). Under acidic conditions (pH 5.2), MBP-ERp44 specifically interacted with GST-1L3V (Figure 2B), but no interaction was observed under neutral (pH 7.2) conditions (data not shown). The pH in the ER lumen has been estimated to be almost neutral (Kim et al., 1998; Foyouzi-Youssefi et al., 2000). We reasoned that certain factor(s) may have been missed in our pulldown assays and attempted to identify conditions under which 1L3V and ERp44 interact at neutral pH.

The presence of THD in ERp44 suggests that its function is redox dependent. Both GST-1L3V and ERp44 were predominantly in their oxidized forms, and addition of the reducing reagent dithiothreitol (DTT) reduced both according to their migration patterns on SDS-PAGE under nonreducing conditions (Figure 2C). No interaction between these oxidized forms was observed at pH 7.5 (Figure 2C, lane 1), while the reduced forms did interact (Figure 2C, lane 2). It was thus concluded that ERp44 and 1L3V bind to each other in a redox-dependent manner at neutral pH.

To determine which of the protein redox states is important, the cysteine residues of the proteins were mutated. Mutation of Cys2496, Cys2504, or Cys2527 of 1L3V resulted in decreased interaction with ERp44 (Figure 2D), whereas no cysteine mutations in ERp44 affected the interaction (Supplemental Figure S2 on the *Cell* website). Taken together, these findings strongly suggest that the presence of free thiol groups in 1L3V is required for the interaction between 1L3V and ERp44 at neutral pH.

We next examined whether the interaction between ERp44 and 1L3V is dependent on the Ca^{2+} concentration. As shown in Figure 2E, the interaction diminished when the Ca^{2+} concentration was higher than 100 μM. The $[Ca^{2+}]_{ER}$ under resting conditions has been estimated to be 200–1000 μM (Meldolesi and Pozzan, 1998), suggesting that the interaction between ERp44 and IP_3R1 is enhanced when $[Ca^{2+}]_{ER}$ is decreased.

The above findings suggested that reducing and/or low $[Ca^{2+}]_{ER}$ conditions favor the interaction between ERp44 and IP_3R1. To corroborate these observations in vivo, COS-7 cells expressing HA-ERp44 and GFP-IP_3R1 were cultured in the presence or absence of DTT, and IP was performed with whole-cell lysates. Although the amount of HA-ERp44 that precipitated with anti-HA antibody was consistently less under reducing conditions for unknown reasons (Figure 2F, bottom panel), coprecipitated GFP-IP_3R1 was significantly increased (Figure 2F, middle panel). In a similar manner, cells expressing HA-ERp44 and GFP-IP_3R1 were stimulated with 10 μM (suprathreshold concentration) ATP, an activator of purinergic receptors, and the stimulation increased the amount of GFP-IP_3R1 that coprecipitated with HA-ERp44 (Figure 2G). Furthermore, Ca^{2+} depletion from the ER, elicited by thapsigargin (Tg, a SERCA inhibitor), also augmented the interaction (Figure 2H). These results indicated that dynamic changes in the ER lumenal environment affect the interaction between IP_3R1 and ERp44.

Next, to gain greater insight into the nature of the interaction, we identified the minimum 1L3V-interacting

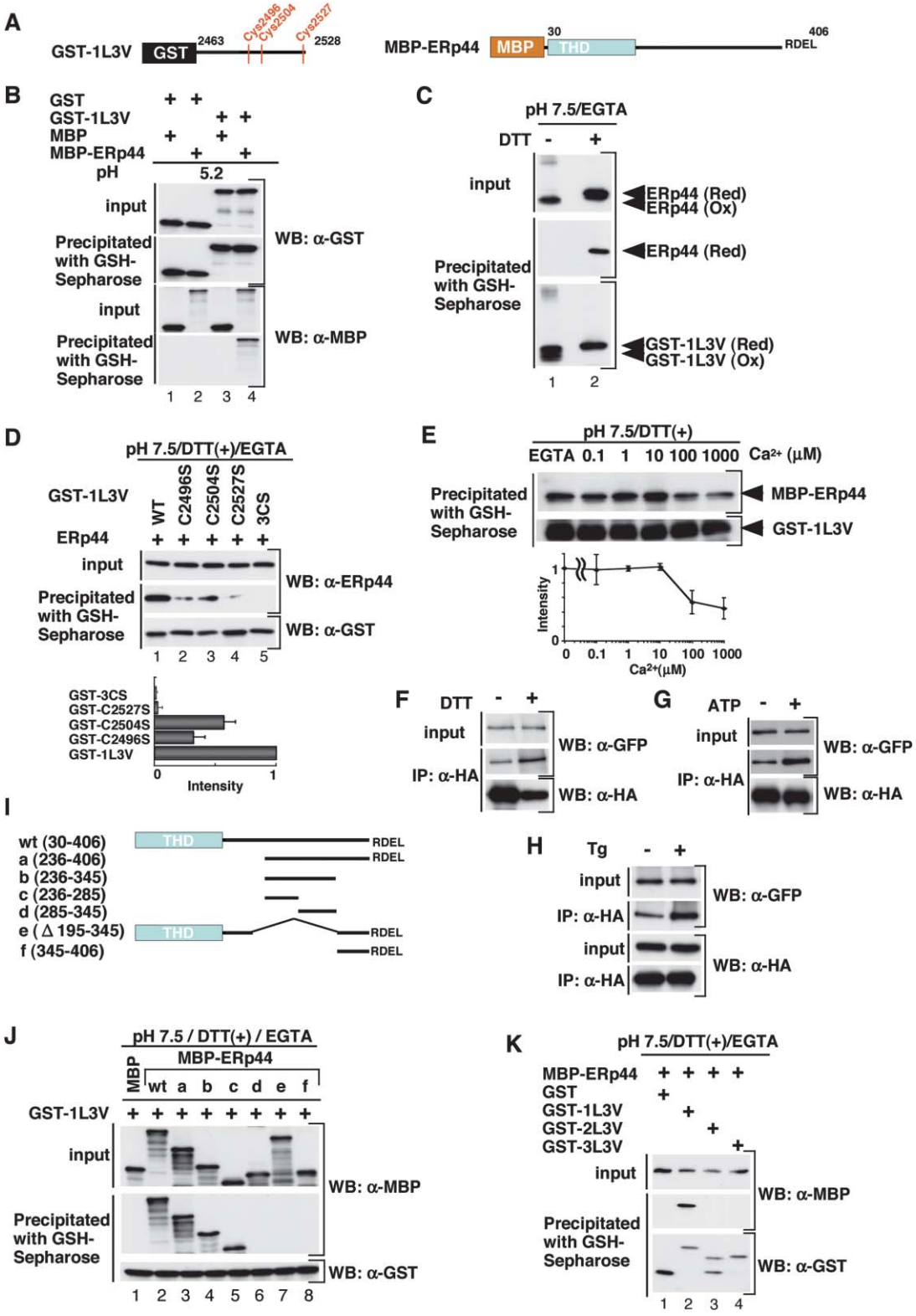

Figure 2. ERp44 Specifically Interacts with IP_3R1 in a Condition-Dependent Manner

(A) Schematic representation of recombinant proteins.

(B) ERp44 directly interacts with 1L3V in acidic buffer. Purified GST (lanes 1 and 2) or GST-1L3V (lanes 3 and 4) was incubated with purified MBP (lanes 1 and 3) or MBP-ERp44 (lanes 2 and 4) in acidic solution (pH 5.2) containing 4 mM Ca^{2+} and then precipitated with GSH-Sepharose. Precipitated proteins were subjected to Western blotting with α-GST or α-MBP.

(C) ERp44 directly interacts with 1L3V in the presence of DTT and EGTA in neutral buffer. To obtain untagged ERp44, purified GST-ERp44

region of ERp44 by fusing the full-length (without the signal sequence) or subfragments of ERp44 to MBP and testing their interactions with GST-1L3V in the presence of DTT at neutral pH. Wild-type MBP-ERp44 and MBP-ERp44 (the C-terminal half) strongly interacted with GST-1L3V (Figure 2J, lanes 2 and 3, respectively), indicating that THD is not required for the interaction. MBP-ERp44c, which contains a highly conserved glutamate-rich region but is devoid of the histidine-rich region, also bound to GST-1L3V, albeit somewhat weakly (Figure 2J, lane 5), whereas other mutants tested did not (Figure 2J, lanes 6–8). These results indicate amino acid residues 236–285 of ERp44 to be necessary and sufficient for binding to 1L3V. The primary sequence of this region has no similarities to any sequences in the database but is well conserved among species (Supplemental Figure S3 on the *Cell* website).

Finally, MBP-ERp44 interacted with GST-1L3V, but not with GST-2L3V or GST-3L3V (Figure 2K), which is consistent with the results of the initial screening with L3V-Fc and the IP experiment (Figures 1C and 1F, respectively). Based on all of the above findings, it was concluded that ERp44 directly interacts with the L3V domain of IP_3R1 in a subtype-specific and ER lumenal environment-dependent manner.

Expression of ERp44 Inhibits IICR via IP_3R1

To explore the functional consequences of ERp44 binding to IP_3R1, we performed Ca^{2+}-imaging experiments with the fluorescent Ca^{2+} indicator fura-2. First, we tested HeLa cells, approximately half of whose IP_3Rs are IP_3R1 (Hattori et al., 2004). Red fluorescent protein (RFP)-tagged ERp44 (RFP-ERp44) or RFP with an ER retention signal (RFP-RDEL, negative control) was then expressed in HeLa cells, and the cells were stimulated with ATP in Ca^{2+}-free medium. In nonexpressing cells, ATP (3 μM) typically caused a single Ca^{2+} transient, occasionally with small oscillations (Figure 3A, black trace), and the response of the cells expressing RFP-RDEL was indistinguishable from that of the nonexpressing cells (Figure 3A, red trace). Cells expressing RFP-ERp44, on the other hand, typically exhibited significantly smaller Ca^{2+} transients (Figure 3B, red trace), and the average peak amplitude in cells expressing RFP-ERp44 was significantly smaller (69.3% $\pm$ 1.8%, $p < 0.05$) than that in the nonexpressing cells (Figure 3C). The difference was not due to a decrease in releasable Ca^{2+} in the ER because the amount of the passive Ca^{2+} leakage elicited by Tg was unchanged (Figures 3D and 3E). Also, IP_3 production was not influenced by overexpression of ERp44 (data not shown).

Next, we tested the effect of ERp44 overexpression in COS-7 cells because they are known to express no IP_3R1 (Boehning and Joseph, 2000; Hattori et al., 2004). Stimulation of cells expressing RFP-RDEL with 1 μM ATP typically elicited a single Ca^{2+} transient (Figure 3F), while expression of RFP-ERp44 had no effect on the pattern or amplitude of the transient (Figures 3G and 3H). No effect of RFP-ERp44 expression was observed when cells were stimulated with lower ATP concentrations (0.3 μM) (data not shown).

The above results suggest that ERp44 inhibits IP_3R1 but does not inhibit IP_3R2 or IP_3R3. To further confirm this, we needed to compare cells that express IP_3R1 only to those expressing no IP_3R1. This was achieved by employing DT40-KMN60 and DT40-1KO cells, both of which were derived from the same parent cell line, DT40 cells. The DT40-KMN60 cell line was established by stably transfecting the mouse IP_3R1 gene on a background of IP_3R-deficient DT40 cells (DT40-TKO, Sugawara et al., 1997). DT40-1KO cells express IP_3R2 and IP_3R3, but not IP_3R1 (Sugawara et al., 1997). Crosslinking of the B cell antigen receptor (BCR) activates PLC-γ, which results in production of IP_3 in DT40 cells. The peak amplitude of BCR-induced Ca^{2+} release in DT40-KMN60 cells expressing RFP-RDEL was approximately the same (96% $\pm$ 2.9%) as in nonexpressing cells (Figure 3K), but it was significantly smaller in DT40-KMN60 cells expressing RFP-ERp44 (60.6% $\pm$ 9.6%, Figures 3I and 3K). There was no reduction in Tg-induced Ca^{2+} leakage

---

was cleaved by thrombin and the GST released then was removed by incubation with GSH-Sepharose. This ERp44 protein was incubated with GST-1L3V in neutral solution (pH 7.5) containing 5 mM EGTA in the presence or absence of 3 mM DTT. The inputs and bead bound proteins were resolved with SDS-PAGE under nonreducing conditions and analyzed by Western blotting with α-ERp44 (top and middle) or α-GST (bottom).

(D) Purified GST-1L3V (lane 1) and its cysteine mutants, C2496S (lane 2), C2504S (lane 3), C2527S (lane 4), and 3CS (C2496S/C2504S/C2527S, lane 5), were incubated with ERp44 (as prepared in [C]) in the presence of 3 mM DTT and 5 mM EGTA. Proteins were then precipitated with GSH-Sepharose and subjected to Western blotting with α-ERp44 (middle) or α-GST (bottom). The amount of ERp44 added to the binding reaction is shown at the top. The histogram depicts densitometric analyses from five independent experiments.

(E) Ca^{2+} dependency of the interaction between 1L3V with ERp44. A binding assay was performed with 3 mM DTT in the presence of EGTA or the Ca^{2+} concentration indicated. Proteins bound to GSH-Sepharose were subjected to Western blotting with α-MBP (top) or α-GST (bottom).

(F) In vivo interaction between IP_3R1 and ERp44 is enhanced under reducing conditions. COS-7 cells expressing GFP-IP_3R1 and HA-ERp44 were treated with 5 mM DTT for 30 min (+) or not (−), then treated with DSP, and IP was performed. The lysates and IP samples were analyzed by Western blotting with α-GFP (top and middle) or α-HA (bottom).

(G and H) In vivo interaction between IP_3R1 and ERp44 is enhanced after ER Ca^{2+} depletion. COS-7 cells expressing GFP-IP_3R1 and HA-ERp44 were stimulated with 10 μM ATP (+) or not (−) for 5 min (G), or 2 μM Tg (+) or not (−) for 30 min (H), treated with DSP, and finally IP was performed. The lysates and IP samples were analyzed by Western blotting with α-GFP or α-HA.

(I) Schematic representation of ERp44 and its mutants.

(J) Amino acid residues 236–285 of ERp44 are responsible for interaction with 1L3V. GST-1L3V was incubated with MBP (lane 1) or MBP fusion proteins containing subfragments of ERp44 (lanes 2–8). Binding assay was performed as in (E). The "control" MBP protein (lane 1) is in fact MBP plus 94 unrelated amino acids derived from the vector (pMAL-c) sequence and its molecular weight is thus larger than those of some ERp44-fusion proteins.

(K) ERp44 specifically interacts with the L3V of IP_3R1, but not that of IP_3R2 or IP_3R3. Purified GST (lane 1), GST-1L3V (lane 2), GST-2L3V (lane 3), or GST-3L3V (lane 4) was incubated with MBP-ERp44 in neutral solution (pH 7.5) containing EGTA and DTT. Proteins bound to GSH-Sepharose were subjected to Western blotting with α-MBP (top and middle) or α-GST (bottom).

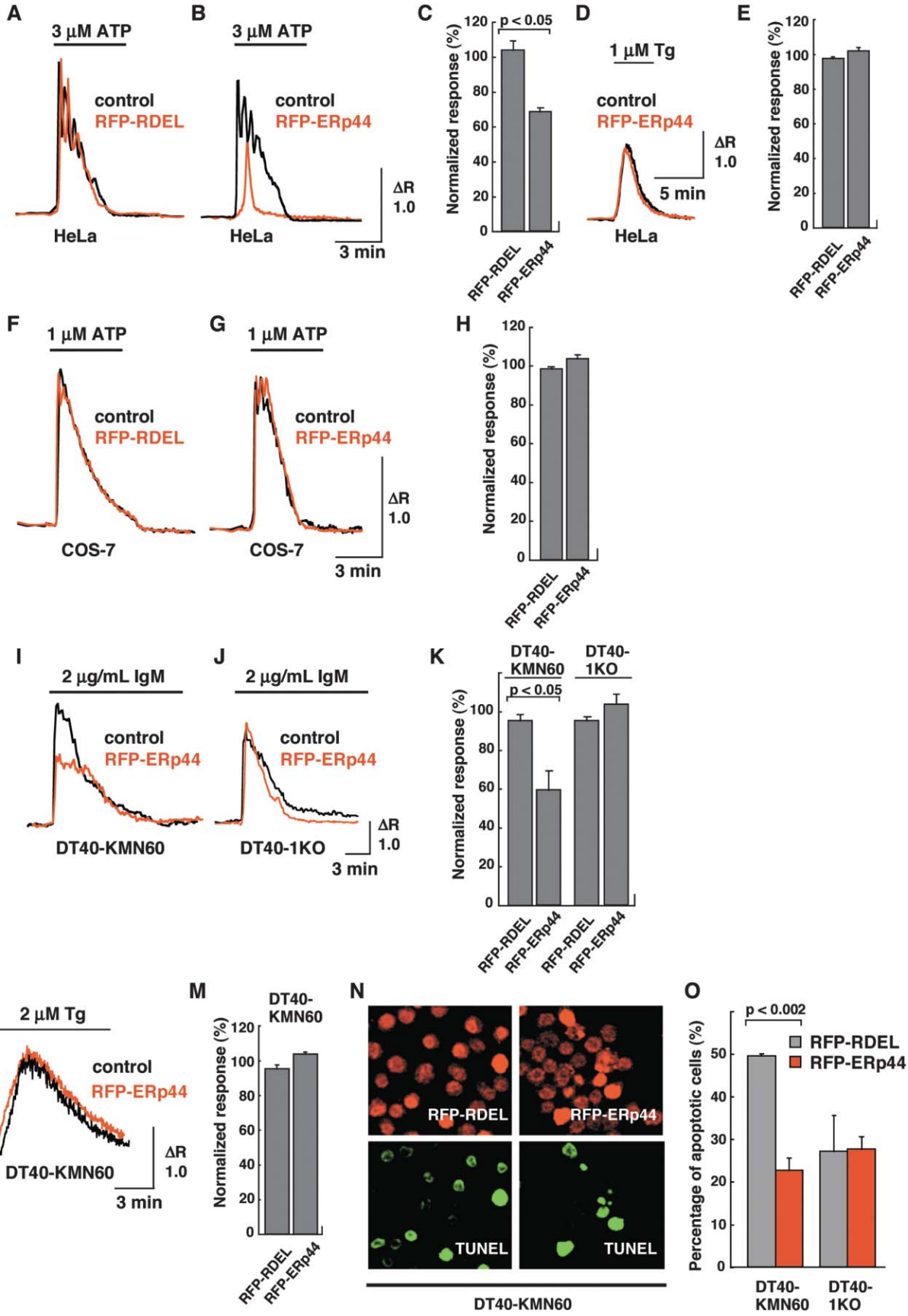
A
3 μM ATP
control
RFP-RDEL
HeLa
B
3 μM ATP
control
RFP-ERp44
HeLa
ΔR
1.0
3 min
C
p < 0.05
Normalized response (%)
120
100
80
60
40
20
0
RFP-RDEL
RFP-ERp44
D
1 μM Tg
control
RFP-ERp44
ΔR
1.0
5 min
HeLa
E
Normalized response (%)
120
100
80
60
40
20
0
RFP-RDEL
RFP-ERp44
F
1 μM ATP
control
RFP-RDEL
COS-7
G
1 μM ATP
control
RFP-ERp44
COS-7
ΔR
1.0
3 min
H
Normalized response (%)
120
100
80
60
40
20
0
RFP-RDEL
RFP-ERp44
I
2 μg/mL IgM
control
RFP-ERp44
DT40-KMN60
J
2 μg/mL IgM
control
RFP-ERp44
DT40-1KO
ΔR
1.0
3 min
K
DT40-KMN60
DT40-1KO
p < 0.05
Normalized response (%)
100
80
60
40
20
0
RFP-RDEL
RFP-ERp44
RFP-RDEL
RFP-ERp44
L
2 μM Tg
control
RFP-ERp44
DT40-KMN60
ΔR
1.0
3 min
M
DT40-KMN60
Normalized response (%)
120
100
80
60
40
20
0
RFP-RDEL
RFP-ERp44
N
RFP-RDEL
RFP-ERp44
TUNEL
TUNEL
DT40-KMN60
O
p < 0.002
RFP-RDEL
RFP-ERp44
Percentage of apoptotic cells (%)
50
40
30
20
10
0
DT40-KMN60
DT40-1KO

in these cells (Figures 3L and 3M). In DT40-1KO cells, on the other hand, expression of RFP-ERp44 had little effect on the peak amplitude (Figures 3J and 3K). These results indicate that ERp44 inhibits IP_3R1, but not IP_3R2 or IP_3R3.

IP_3Rs have a critical function in BCR-induced apoptosis in DT40 cells (Sugawara et al., 1997). We found that expression of REP-ERp44, but not RFP-RDEL, significantly inhibited apoptosis in DT40-KMN60 cells (Figures 3N and 3O), but no such effect was observed in DT40-1KO cells (Figure 3O), implying that inhibition of IP_3R1 by ERp44 affects cell functions, such as apoptosis.

Specific Knockdown of ERp44 Results in Augmentation of IICR via IP_3R1

Next, we used the RNA interference technique to investigate the role of endogenous ERp44 by testing two different small interfering RNA (siRNA) sequences targeted to the open reading frame (siERp44-ORF) and the 3′-untranslated region (siERp44-3U), respectively, of human ERp44. To provide negative controls, we introduced three-point mutations in these siRNAs (siControl-ORF or siControl-3U, respectively). Western analysis revealed both siERp44-ORF and siERp44-3U to efficiently and specifically "knock down" ERp44 in HeLa and COS-7 cells (Figure 4A). Unfortunately, however, none of the siRNAs targeted to chicken ERp44 decreased the amount of ERp44 in DT40 cells (data not shown). In HeLa cells, knockdown of ERp44 neither affected the expression of other ER oxidoreductases nor induced unfolded protein response within 48 hr (Supplemental Figure S5 online).

SiRNA-transfected HeLa cells were stimulated with 1, 3, and 10 μM ATP. Stimulation with 1 μM ATP rarely (4.0% ± 0.3% of all cells) evoked discernible Ca^{2+} signals in siControl-3U-transfected cells (Figures 4B and 4C, black trace and bar), whereas approximately five times the number (20.1% ± 2.5%) of siERp44-3U-transfected cells responded (Figures 4B and 4C, red trace and bar). Subsequent stimulation with 3 μM ATP elicited IICR in 46.9% ± 1.6% of the control cells and 90.3% ± 1.2% of the cells transfected with siERp44-3U (Figures 4B and 4C), whereas most of the cells in both preparations responded when stimulated with 10 μM ATP (Figure 4C). The average peak amplitude was higher in siERp44-3U-transfected cells than in the siControl-3U-transfected cells at all ATP concentrations (Figure 4D). These ERp44 knockdown effects were confirmed to be specific by transfecting the cells with RFP-ERp44 ("rescue" experiments, Supplemental Figure S4). Knockdown of ERp44 had no effect on the Ca^{2+} leakage induced by Tg (data not shown).

We then performed the same experiments in COS-7 cells. Since COS-7 cells do not express IP_3R1, we predicted that knockdown of ERp44 would have no effect on IICR in this cell line, and the results confirmed our prediction (Figures 4E–4G). These findings indicate that ERp44 specifically inhibits IP_3R1.

Cysteine Residues in the L3V Domain Are Important for Inhibition of IP_3R1 Activity by ERp44

Next, we investigated the significance of the cysteine residue(s) in 1L3V in terms of the inhibition of IP_3R1 by ERp44. We first investigated whether mutations of these residues in full-length (and GFP-tagged) IP_3R1 affected IICR activity (Figure 5A). When Cys2527, which is located adjacent to the channel pore region, was mutated, channel activity was completely lost (Figure 5A), and this mutant was not used any further. Mutations in Cys2496 and Cys2504, however, had no effect on channel activity (Figure 5A). Interaction between these IP_3R1 mutants and ERp44 was significantly decreased (Figure 5B), consistent with the results obtained with recombinant proteins (Figure 2D). The IP_3R1 mutant was cotransfected into DT40-TKO cells with either RFP-RDEL or RFP-ERp44, and a Ca^{2+}-imaging experiment was performed. IICR via GFP-IP_3R1 (i.e., wild-type) was suppressed by coexpression with RFP-ERp44, but not with RFP-RDEL (Figures 5C and 5F). Surprisingly, this inhibition by ERp44 was almost completely abolished by substitution of the Cys2496 or Cys2504 of GFP-IP_3R1 (Figures 5D and 5E, respectively, and Figure 5F). These results clearly demonstrated that the presence of free thiol groups in the L3V domain is important for inhibition of IP_3R1 by ERp44.

ERp44 Inactivates Channel Activity of IP_3R1 in Lipid-Bilayer System

To unambiguously demonstrate that ERp44 inhibits IP_3R1, we performed single-channel current recording

Figure 3. Expression of ERp44 Inhibits IICR in HeLa and DT40-KMN60 Cells, but Not in COS-7 or DT40-1KO Cells

(A and B) ERp44 inhibits IICR in HeLa cells. Cells transfected with either RFP-RDEL (A) or RFP-ERp44 (B) were stimulated with 3 μM ATP. Representative Ca^{2+} responses in nonexpressing (black) and expressing cells (red) are shown.

(C) Quantitation of results in (A) and (B). Normalized responses were calculated with the averaged peak amplitude of nonexpressing cells set equal to 100%. $p < 0.05$ compared to RFP-RDEL (Student's t test).

(D) The Ca^{2+} storage capacity is unchanged in HeLa cells expressing RFP-ERp44. Cells were stimulated with 1 μM Tg, and representative Ca^{2+} responses in nonexpressing (black) and expressing cells (red) are shown.

(E) Quantitation of the results in (D).

(F–H) ERp44 does not affect IICR in COS-7 cells. Cells transfected with either RFP-RDEL (F) or RFP-ERp44 (G) were stimulated with 1 μM ATP. Representative Ca^{2+} responses in nonexpressing (black) and expressing cells (red) are shown.

(H) Quantitation of results shown in (F) and (G).

(I–K) ERp44 inhibits IICR in DT40-KMN60 but not in DT40-1KO cells. Cells were stimulated with 2 μg/ml anti-IgM. Representative Ca^{2+} responses in nonexpressing (black) and expressing cells (red) are shown, and their quantitations are shown in (K).

(L and M) ERp44 does not affect Ca^{2+} storage capacity in DT40-KMN60 cells. Ca^{2+} responses in nonexpressing (black) and expressing cells (red) and their quantitations are shown in (M).

(N and O) ERp44 inhibits BCR-induced apoptosis in DT40-KMN60 cells, but not in DT40-1KO cells. Cells were treated with anti-IgM (2 μg/ml) for 24 hr and apoptosis was assessed by TUNEL assay. Data are TUNEL-positive cells as a percentage of all cells expressing RFP-RDEL (gray) or RFP-ERp44 (red) from two independent experiments. $p < 0.002$ compared with RFP-RDEL (Student's t test).

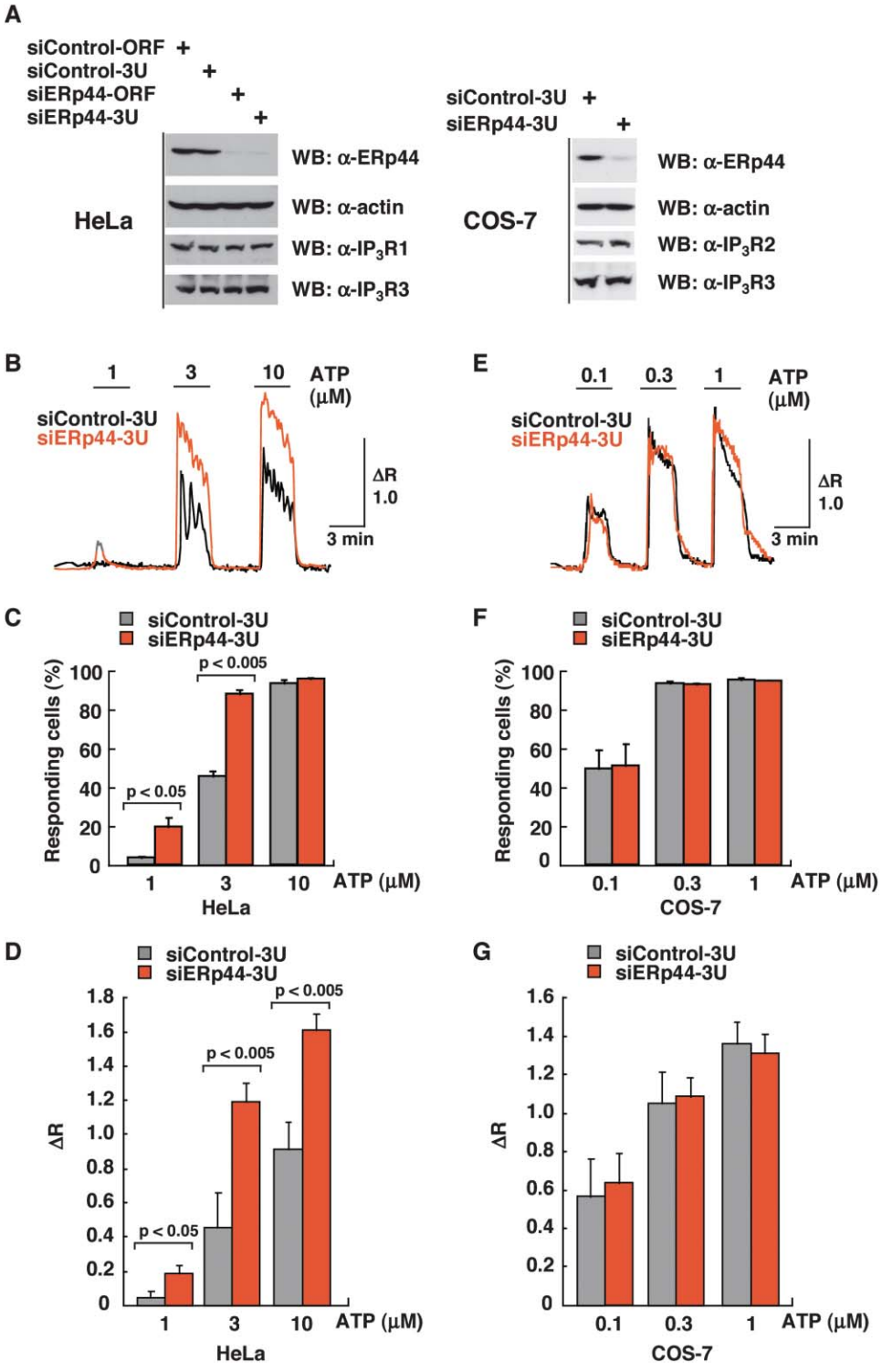

Figure 4. Knockdown of ERp44 Augments IICR in HeLa Cells, but Not in COS-7 Cells

(A) Knockdown of ERp44 in HeLa and COS-7 cells. The lysates of HeLa (left) and COS-7 cells (right) transfected with the siRNA indicated were analyzed by Western blotting with the antibodies indicated.

(B) Knockdown of ERp44 augments IICR in HeLa cells. Cells were stimulated with 1, 3, and 10 μM ATP in the presence of extracellular Ca^{2+}. Representative Ca^{2+} responses in siControl-3U-transfected (black) or siERp44-3U-transfected cells (red) are shown.

(C) Percentages of HeLa cells transfected with siControl-3U (gray) or siERp44-3U (red) that showed discernible Ca^{2+} responses at the ATP concentrations indicated.

(D) Average peak amplitude of the Ca^{2+} response in HeLa cells transfected with siControl-3U (gray) or siERp44-3U (red).

(E) COS-7 cells were stimulated with 0.1, 0.3, and 1 μM ATP in the presence of extracellular Ca^{2+}. Representative Ca^{2+} responses in siControl-3U-transfected (black) and siERp44-3U-transfected cells (red) are shown.

(F) Percentages of COS-7 cells transfected with siControl-3U (gray bars) or siERp44-3U (red bars) that showed discernible Ca^{2+} responses at the ATP concentrations indicated.

(G) Average peak amplitude of the Ca^{2+} response in COS-7 cells transfected with siControl-3U (gray columns) or siERp44-3U (red columns).

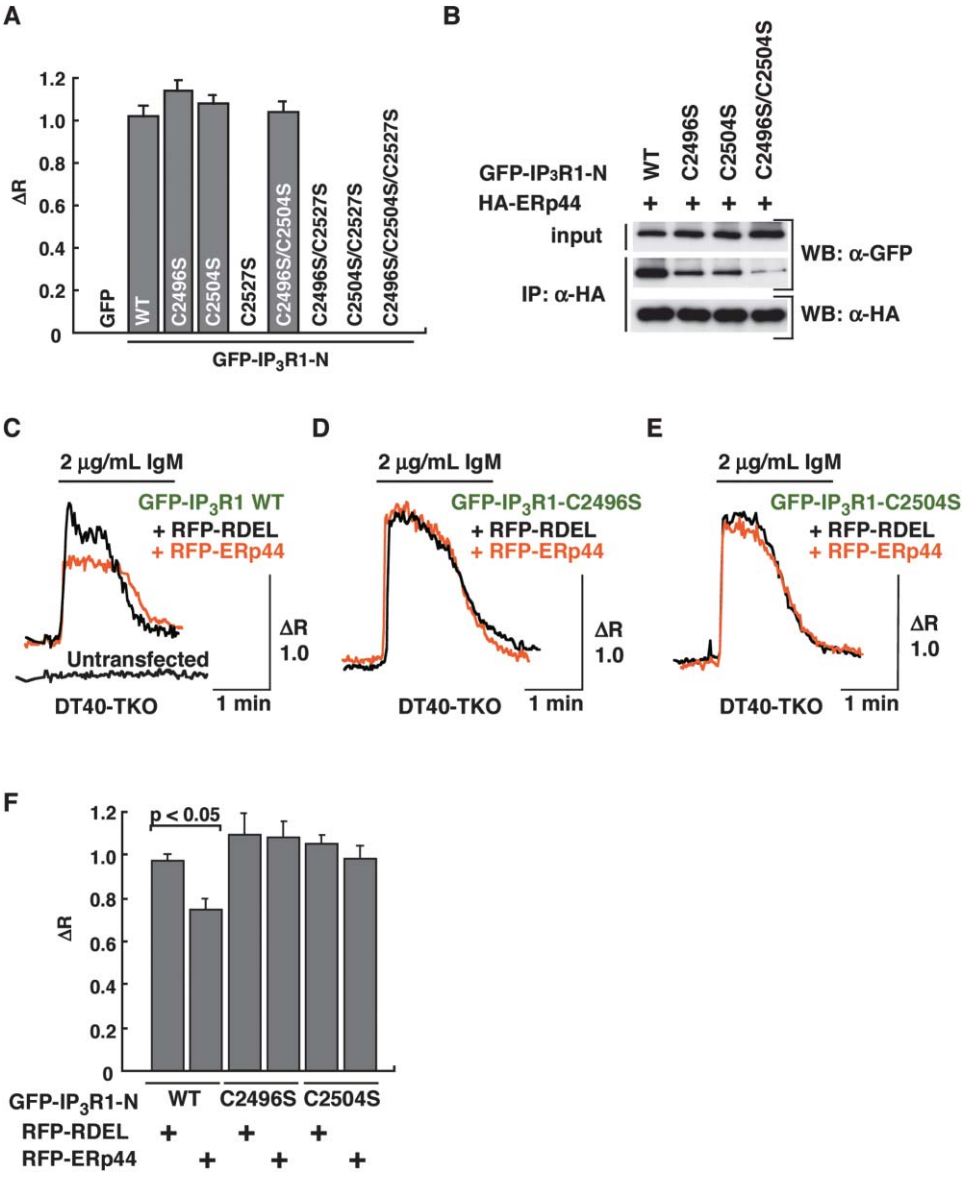

Figure 5. Cysteine Residues of 1L3V Are Required for Inhibition of IP_3R1 by ERp44

(A) DT40-TKO cells expressing GFP, GFP-IP_3R1, or GFP-IP_3R1 with cysteine replacements were stimulated with 2 μg/ml anti-IgM. Average peak amplitudes of the Ca^{2+} response are shown.

(B) Cysteine residues of the L3V domain of IP_3R1 are important for interaction between IP_3R1 and ERp44. GFP-IP_3R1 or its cysteine mutant was transfected with HA-ERp44 in COS-7 cells. Thirty-six hours after transfection, the cells were treated with DSP, and IP was performed with anti-HA. The lysates and IP samples were analyzed by Western blotting with α-GFP (top and middle) or α-HA (bottom).

(C–E) ERp44 inhibits IICR in DT40-TKO cells expressing IP_3R1, but not in cells expressing IP_3R1 cysteine mutants. RFP-RDEL or RFP-ERp44 was transfected into DT40-TKO cells with GFP-IP_3R1 or its cysteine mutant. Thirty-six hours after transfection, the cells were stimulated with 2 μg/ml anti-IgM. Representative Ca^{2+} responses in RFP-RDEL-expressing (black) and RFP-ERp44-expressing cells (red) are shown.

(F) Summary of the Ca^{2+}-imaging experiments in (C)–(E). Average peak amplitudes of the ratios are shown.

in a planar lipid bilayer fused with mouse cerebellar microsomes in which 99% of the IP_3Rs are IP_3R1 (Taylor et al., 1999). We first confirmed the interaction between MBP-ERp44 and GST-1L3V in the lumenal-side solution containing 3 mM DTT (Figure 6A). IP_3R1 activity was recorded with Ba^{2+} as a charge carrier in the presence of 3 mM DTT in the trans (lumenal) compartment. Addition of MBP-ERp44 resulted in inhibition of the channel activity in a dose-dependent manner (Figures 6B–6E), but addition of MBP (negative control) to the lumenal compartment had no effect on IP_3R1 activity (data not shown). Whether or not addition of more MBP-ERp44 can completely block the channel activity was not testable since we were unable to obtain a more concentrated recombinant ERp44 protein and adding more of the solution had nonspecific effects on channel activity (data not shown). ERp44 decreased the frequency of channel opening, but did not affect the mean open time of the channel (1.6 ± 0.5 ms and 1.5 ± 0.7 ms [mean ± SD, n = 6] before and after addition of 7.5 μM MBP-ERp44,

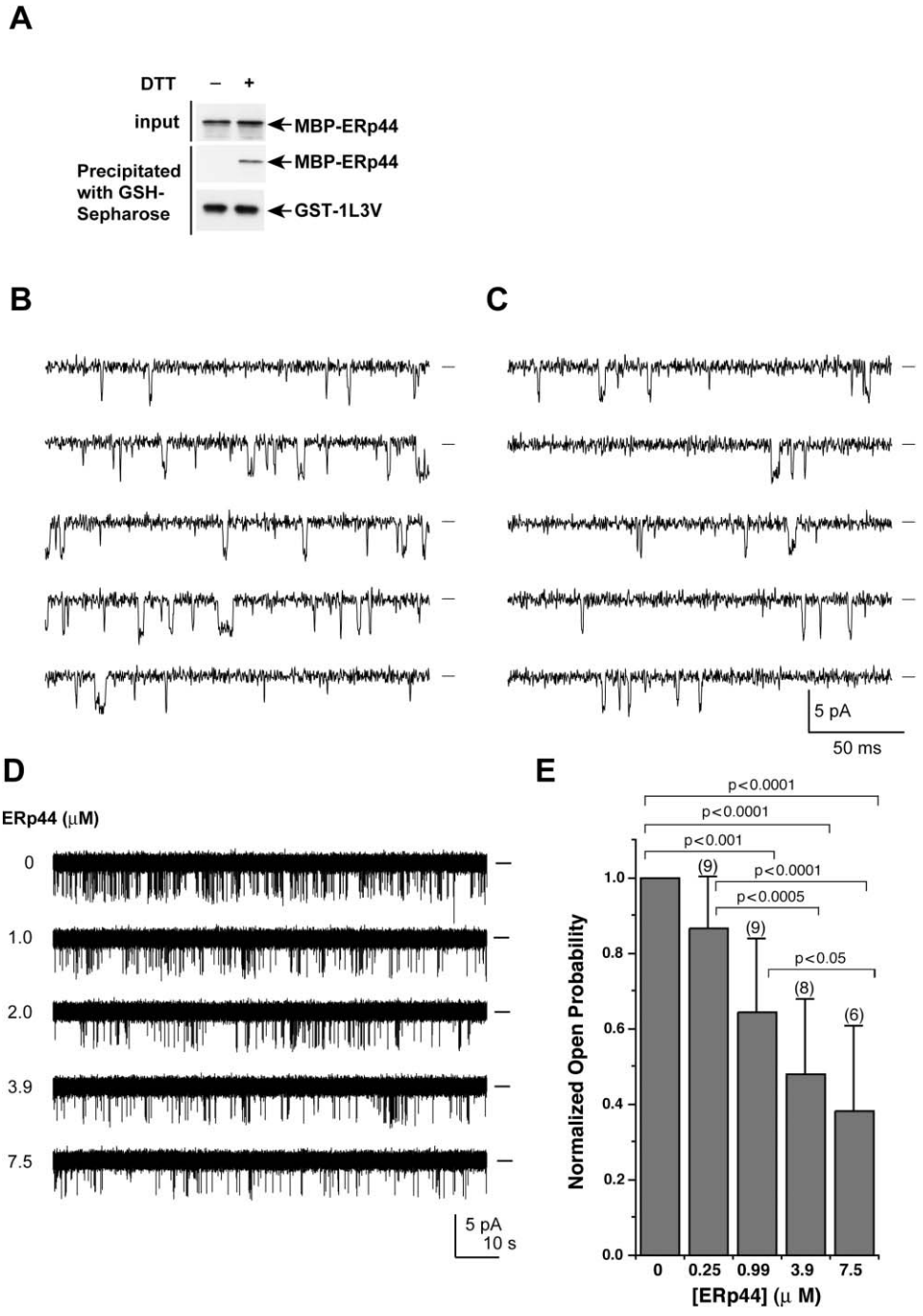

Figure 6. ERp44 Inhibits IP_3R1 in a Lipid Bilayer System

(A) MBP-ERp44 and GST-1L3V were incubated in the *trans* solution with (+) or without (−) 3 mM DTT and then precipitated with GSH-Sepharose. Precipitated proteins were analyzed by Western blotting.

(B and C) Sequential records before (B) and after addition (C) of 7.5 μM MBP-ERp44. Channels were recorded at −20 mV. Continuous 1 s records filtered at 1 kHz are shown.

(D) Effects of ERp44 on single-channel activity of IP_3R1 in the presence of 6.4 μM cytosolic (*cis*) IP_3 and 3 mM lumenal (*trans*) DTT. Serial additions of purified MBP-ERp44 were made to the lumenal compartment. Channel openings are shown as downward deflections from baseline (denoted by the horizontal lines). The data shown are representative of six independent experiments. Data were filtered at 0.5 kHz. The absolute values of open probability before the addition of ERp44 were in the 0.008–0.086 range.

(E) Dose-dependent inactivation of IP_3R1 by ERp44 under lumenal reducing conditions. The averages of open probabilities were normalized to the maximum IP_3R1 activity observed in each experiment. The data are means ± SD. Statistical analysis was done using repeated measures one-way ANOVA with Bonferoni's post-hoc tests. The number of independent trials is indicated above each bar.

respectively), indicating that ERp44 modulated the closed state of IP_3R1. Similarly, addition of ERp44 did not alter the amplitude of the single-channel current (3.7 ± 0.2 pA and 3.6 ± 0.2 pA [mean ± SD, n = 6] at −20 mV before versus after addition of MBP-ERp44, respectively). Raising the IP_3 concentration to 25 μM did not reverse the inhibitory effect of MBP-ERp44, and there was no indication that MBP-ERp44 lowers the IP_3 sensitivity of IP_3R1 (data not shown). No inactivation was observed in the absence of DTT (data not shown), further supporting the hypothesis that the free thiol group(s) in the L3V domain are involved in inhibition by ERp44. These bilayer studies revealed that ERp44 functions to maintain the closed state of IP_3R1 rather than affecting the characteristics of its open state.

Discussion

In this study we demonstrated that ERp44 directly interacts with the L3V domain of IP_3R1, thereby inhibiting its channel activity. This functional interaction is dependent on the pH, redox state, and $[Ca^{2+}]_{ER}$. It is particularly noteworthy that cysteine residues in the L3V domain of IP_3R1 play critical roles in both interaction with and inhibition by ERp44. This is the first example of a negative regulator of IP_3Rs on the ER lumen side and provides support for the hypothesis that IP_3Rs are specifically controlled by the intralumenal, in addition to by the cytosolic, environment.

Roles of Redox State, $[Ca^{2+}]_{ER}$, and pH in Dynamic Regulation of IP_3R by ERp44

It is widely accepted that the ER lumen is more oxidizing than the cytosol, and the ratio of reduced to oxidized glutathione in the ER lumen has been estimated to be from 3:1 to 1:1 (Hwang et al., 1992; Bass et al., 2003), suggesting that roughly 50%–75% of all lumenal cysteine residues are in the reduced (free thiol) form. However, it is also known that some proteins are either exclusively in the oxidized or the reduced state. While the mechanisms that control the redox state of extracellular proteins and ER oxidoreductases are being clarified (Sevier and Kaiser, 2002), how the redox state of other ER resident proteins (including IP_3Rs) is regulated is poorly understood. Our results indicate that the interaction between ERp44 and 1L3V weakens as the number of free thiol groups on 1L3V decreases (Figures 2D, 2F, and 5B). Therefore, if the cysteine residues of an IP_3R1 tetramer form a disulfide bond or are modified by, for example, nitrosylation, it would not bind to ERp44. Based on all of the evidence considered, we hypothesize that some of the cysteine residues in the L3V domain of IP_3R1 are in their free (reduced) form and that others have formed disulfide bonds or are modified. The disulfide bonds may be formed in the same polypeptide, between subunits, or with other molecules. IP_3R1 that have free cysteine residues in the L3V domain are subject to inhibition by ERp44. It must be pointed out that the number and approximate positions of cysteine residues are conserved in all IP_3R subtypes (Figure 1B), raising the possibility that forming a heterotetramer with these subtypes by disulfide bonds may be one way that the IP_3R1 polypeptide escapes inhibition. Whether the redox state, modification, or disulfide bond formation of these cysteine residues is controlled by a specific mechanism is a crucial and challenging question.

Previous studies have shown IICR to be diminished at low $[Ca^{2+}]_{ER}$, and this finding cannot be fully explained by the decreased Ca^{2+} concentration gradient across the ER membrane (e.g., Caroppo et al., 2003). Since the interaction between ERp44 and IP_3R1 is weaker when $[Ca^{2+}]_{ER}$ exceeds 100 μM (i.e., at resting levels, Figure 2E), it is tempting to speculate that the inhibition of IICR previously observed at low $[Ca^{2+}]_{ER}$ is due to enhanced binding of ERp44 to IP_3R1. More detailed investigation at both the cellular and the single-channel level is necessary to resolve this issue.

The pH in the ER lumen has been considered to be almost neutral and stable even during and after Ca^{2+} release (Foyouzi-Youssefi et al., 2000; Kim et al., 1998). However, it is also known that the pH in the lumen of the sarcoendoplasmic reticulum changes drastically after Ca^{2+} release (Kamp et al., 1998), and oligodendrocytes (glial cell type that have long and branched protrusions like neurons) have pH "microdomains," some of which could be below 6.5 (Ro and Carson, 2004). Thus, the pH in the ER lumen may also change in certain cell types or under certain conditions, and in such cases IP_3R1 may be more subject to inhibition by ERp44.

Physiological Significance of IP_3R1 Inhibition by ERp44

Central neurons express exclusively IP_3R1 (Taylor et al., 1999) and it is well known that localized Ca^{2+} release plays a variety of roles in these cell types (Berridge, 2002). In view of the fact that ERp44 can regulate IP_3R1 in a microenvironment-dependent manner, it is tempting to hypothesize that ERp44 is involved in the spatiotemporal regulation of localized Ca^{2+} release in neurons. Particularly, as both IICR and the redox state are involved in synaptic modulations (Inoue et al., 1998; Nishiyama et al., 2000; Knapp and Klann, 2002), ERp44 may also function in these processes. In addition, it was recently appreciated that some of the genetic abnormalities that cause neurodegenerative diseases augment IICR (Tang et al., 2003; Stutzmann et al., 2004), which may be the direct cause of neuronal death. Whether these IICR-activating mutations affect the function of ERp44, or even whether ERp44 can counteract them, are important pathological questions.

More generally, since the ER is the intersection of many signaling pathways (Berridge et al., 2003; Orrenius et al., 2003), inhibition of IP_3R1 by ERp44 may be involved in the feedback system by which information that has converged in the ER lumen is conveyed to the cytosol/nucleus in the form of $[Ca^{2+}]_C$. In other words, ERp44 translates the ER lumenal environment into a $[Ca^{2+}]_C$ by modulating IP_3R, and such a mechanism would allow the functions of the ER lumen (e.g., folding and glycosylation) and of the cytosol/nucleus (e.g., phosphorylation signaling and gene expression) to operate in a concerted matter.

Since the functions of many ER lumenal enzymes and chaperones are Ca^{2+} dependent, inhibition of Ca^{2+} release when the $[Ca^{2+}]_{ER}$ falls below the resting level would be consistent with maintaining their functions.

ERp44 was identified as a protein that forms mixed disulfide bonds with Ero1α, an ER oxidoreductase (Anelli et al., 2002), and it was shown to be involved in ER retention of Ero1α (Anelli et al., 2003). The functions of Ero1 family proteins are not fully understood, but since they play pivotal roles in oxidative protein folding (Tu and Weissman, 2002), ERp44 may play dual roles in protein folding: inhibiting Ca^{2+} release (which reinforces Ca^{2+}-dependent chaperones) by inactivating IP_3R1 and supporting disulfide bond formation by reinforcing the Ero1α/oxidoreductase system. The fact that ERp44 is induced during the unfolded protein responses (Anelli et al., 2002) fits well with this model.

Redox-Dependent Regulation of Cellular Ca^{2+} Signaling

It was very recently reported that SERCA 2b activity is modulated by CRT and ERp57, an ER lumenal oxidoreductase, in a $[Ca^{2+}]_{ER}$- and redox state-dependent manner (Li and Camacho, 2004). Since the pump activity of SERCA 2b is higher when thiol groups in its lumenal loop are reduced, when the ER lumenal environment shifts to the reducing condition, Ca^{2+} uptake by SERCA 2b should be enhanced (by ERp57) and Ca^{2+} release via IP_3R1 should be inhibited (by ERp44). In other words, SERCA 2b and IP_3R1 work together to increase $[Ca^{2+}]_{ER}$ under reducing conditions. This is reasonable since a reduced ER lumenal environment is unfavorable for protein folding and increasing $[Ca^{2+}]_{ER}$ benefits the function of the many chaperones and oxidoreductases that require a relatively high $[Ca^{2+}]_{ER}$. Finally, we obtained no indication that ERp57 (or PDI) associates with IP_3R1 (Supplemental Figure S6 online) or that ERp44 associates with SERCA 2b (data not shown).

Future Directions

To learn how ER lumenal conditions regulate the interaction between ERp44 and IP_3R1 and what the consequences of the interaction are in greater detail, it will be necessary to monitor ER lumenal conditions and the $[Ca^{2+}]_C$ in real time. It is also imperative to investigate the effect of ERp44 on IP_3R1 by using the planar lipid bilayer system under various conditions.

Finally, we were unable to find any protein in the brain (where IP_3R1 is exclusively expressed) that binds to the lumenal domain of IP_3R2 or IP_3R3, but these subtypes are likely to have different binding proteins that are not present in the brain. The fact that the cysteine residues in the L3V domain are conserved (Figure 1B) supports this hypothesis. Searching for such interacting protein(s), investigating how the lumenal environment regulates IP_3R2 and IP_3R3, and how it is related to ERp44/IP_3R1 are our next research challenges.

Experimental Procedures

Plasmids

Full-length ERp44 cDNA was obtained from P14 mouse cerebellum by the reverse transcriptase-polymerase chain reaction. The expression vectors for epitope-tagged or fluorescent protein-tagged ERp44, IP_3Rs, and their mutants were constructed by utilizing the polymerase chain reaction. The details of these methods, including the sequences of the primers used, will be supplied on request. All constructs were verified by DNA sequencing.

Antibodies

Rabbit polyclonal antibody to ERp44 was raised to purified His_6-ERp44 and affinity-purified with MBP-ERp44 coupled to CNBr-activated Sepharose 4B (Amersham). Other antibodies used were anti-IP_3R1 18A10, anti-IP_3R3 KM1082 (for both, see Hattori et al., 2004), anti-HA (12CA5, a gift of Dr. T. Yamamoto), anti-HA-Peroxidase (3F10, Roche), anti-CRT (Affinity BioReagents), anti-MBP (New England Biolabs), anti-human IgG (Vector Laboratories), anti-GST (Amersham), anti-GFP, and anti-actin (both Santa Cruz). The hybridoma producing anti-IgM (M-4 clone) was kindly provided by Dr. T. Kurosaki (Kansai Medical University).

Cell Culture and Transfection

COS-7, HeLa, and 293T cells were cultured in Dulbecco's modified Eagle medium supplemented with 10% heat-inactivated fetal bovine serum. DT40 cells were cultured in RPMI1640 medium supplemented with 10% heat-inactivated fetal bovine serum, 1% chicken serum, 100 U/ml penicillin and streptomycin, 2 mM glutamine, and 50 μM 2-mercaptoethanol. HeLa, COS-7, and 293T cells were transfected with expression vectors or siRNAs by means of TransIT (Mirus) or Lipofectamine2000 (Invitrogen). DT40 cells were transfected by electroporation with Nucleofector (Amaxa).

Identification of ERp44

1L3V-Fc or control Fc was expressed in 293T cells. After collecting the medium and incubating it with Protein-G Sepharose (Amersham) for 2 hr at 4°C, the beads were washed with 10 mM Tris-HCl (pH 8.0) and 150 mM NaCl. Approximately 0.2 mg of 1L3V-Fc or control Fc was coupled to beads, and the beads were loaded into a column. P14 mouse cerebella were washed with ice-cold PBS and homogenized in a buffer containing 0.32 M sucrose, 10 mM Tris-HCl (pH 7.5), 2 mM EDTA, and 1 mM DTT. The homogenates were centrifuged for 1 hr at 100,000 × *g* at 2°C, and after solubilizing the pellet in buffer containing 30 mM sodium acetate, 150 mM NaCl, 4 mM $CaCl_2$, and 1% Triton X-100, the solution was centrifuged at 10,000 × *g* for 15 min. The supernatant was applied to affinity columns, and the columns were washed with the same buffer, followed by neutral Ca^{2+} buffer (10 mM Tris-HCl [pH 8.0], 150 mM NaCl, 4 mM $CaCl_2$, and 1% Triton X-100), and finally neutral chelator buffer (10 mM Tris-HCl [pH 8.0], 150 mM NaCl, 5 mM EDTA, 5 mM EGTA, and 1% Triton X-100).

Western Blot Analysis

Proteins were resolved by SDS-PAGE and transferred to a polyvinylidene difluoride membrane. The membranes were blocked with 5% skim milk in PBS containing 0.05% Tween-20 (PBST) for 30 min and probed with the primary antibody for 3 hr at room temperature (RT). After washing with PBST, the membranes were incubated with a suitable secondary antibody and signals were detected with an ECL Plus kit (Amersham).

IP and GST-Pulldown Assay

For IP, cells were washed with PBS and then exposed to 2 mM DSP (Pierce) in PBS for 30 min at RT. After washing with PBS, the cells were solubilized in TNE buffer (150 mM Tris-HCl [pH 7.5], 500 mM NaCl, 1 mM EDTA, 1% Triton X-100, 0.1% SDS), and the lysates were incubated with the antibodies indicated and Protein-G Sepharose for 2 hr at 4°C. The beads were then washed five times with TNE buffer, and the proteins were eluted by boiling in SDS-PAGE sampling buffer.

Recombinant proteins were expressed in *E. coli* BL21 and purified with GSH-Sepharose (Amersham) or Amylose Resin (New England Biolabs). GST or GST fusion proteins were incubated with MBP or MBP fusion proteins for 1 hr at 4°C in acidic solution (30 mM NaOAc [pH 5.2], 150 mM NaCl, 4 mM $CaCl_2$, 0.1% Triton X-100). ERp44 and GST fusion proteins were incubated in neutral buffer (20 mM Tris-HCl [pH 7.5], 150 mM NaCl, 5 mM EGTA, 0.1% Triton X-100) with or without 3 mM DTT. GST-1L3V and MBP-ERp44 were incubated in neutral buffer or neutral buffer in which EGTA had been replaced with $CaCl_2$. The experiments in Figures 2D, 2E, 2J, and 2K were carried out in neutral buffer containing 3 mM DTT.

RNA Interference

SiRNA duplexes were purchased from Dharmacon. The target sequences were siControl-C (5′-AAGUAGUGUAUGCUAGAGUGG-3′), siERp44-C (5′-AAGUAGUGUUUGCCAGAGUUG-3′), siControl-3U (5′-AACAGCACCAUCGACCAACGU-3′), siERp44-3U (5′-AACAGCAGCAUCAACCUACGU-3′).

Ca^{2+} Imaging

At 24–48 hr following transfection, cells were incubated for 30 min with 5 μM fura-2 AM (Dojindo). The cells were then placed on the stage of an inverted microscope (IX-70; Olympus, Japan) and perfused with balanced salt solution (BSS). Image capture and processing were performed with an Argus 50/CA system (Hamamatsu Photonics, Japan) at RT by a standard ratiometric method (excited at 340 nm and 380 nm). Fluorescence images of GFP and RFP were acquired separately and saved in the computer in the same optical fields as the fluorescence images for Ca^{2+} imaging. We also performed Ca^{2+}-imaging experiments using fura-4F AM in all cell types used in this study and confirmed that all of the responses obtained in experiments using fura-2 were not saturated (data not shown).

Planar Lipid Bilayer Experiments

Single-channel recordings of IP_3R1 in mouse cerebellar microsomes were performed as described previously (Michikawa et al., 1999), with some modifications. The *cis* chamber contained 108 mM Tris dissolved in 250 mM HEPES (pH 7.33), 1.11 mM K_2-H-HEDTA (N-hydroxyethylethylenediamine-N,N',N'-triacetic acid), 0.12 mM K-Ca-HEDTA. The *trans* chamber contained 250 mM HEPES (pH 7.33), 53 mM $Ba(OH)_2$, 3 mM DTT. IP_3R1 was activated by the addition of 6.4 μM IP_3 and 0.5 mM ATP to the *cis* chamber. Purified MBP or MBP-ERp44 was added directly to the *trans* side. The currents were amplified (Axon Instruments), filtered at 1 kHz with a low-pass Bessel filter (NF Instruments), and sampled at 10 kHz. Single-channel data were analyzed as described previously (Michikawa et al., 1999).

Acknowledgments

We thank K. Nakamura and A. Suzuki for excellent technical assistance and Dr. T. Inoue for invaluable discussions and technical help. We also thank Drs. A. Miyawaki, H. Bito, T. Shimizu, and A. Mizutani for critical reading of the manuscript. This study was supported by the grant from the JST, and the Grants-in-Aid (M.H. and K.M.) and The 21st Century COE Program, Center for Integrated Brain Medical Science, from the Ministry of Education, Culture, Sports, Science and Technology, Japan.

Received: April 28, 2004
Revised: August 24, 2004
Accepted: November 18, 2004
Published: January 13, 2005

References

Anelli, T., Alessio, M., Mezghrani, A., Simmen, T., Talamo, F., Bachi, A., and Sitia, R. (2002). ERp44, a novel endoplasmic reticulum folding assistant of the thioredoxin family. EMBO J. *21*, 835–844.

Anelli, T., Alessio, M., Bachi, A., Bergamelli, L., Bertoli, G., Camerini, S., Mezghrani, A., Ruffato, E., Simmen, T., and Sitia, R. (2003). Thiol-mediated protein retention in the endoplasmic reticulum: the role of ERp44. EMBO J. *22*, 5015–5022.

Bass, R., Ruddock, L.W., Klappa, P., and Freedman, R.B. (2003). A major fraction of ER-located glutathione is present as mixed disulfides with protein. J. Biol. Chem. *279*, 5257–5262.

Berridge, M.J. (2002). Neuronal calcium signaling. Neuron *21*, 13–26.

Berridge, M.J., Bootman, M.D., and Roderick, H.L. (2003). Calcium signalling: dynamics, homeostasis and remodelling. Nat. Rev. Mol. Cell Biol. *4*, 517–529.

Boehning, D., and Joseph, S.K. (2000). Functional properties of recombinant type I and type III inositol *1*, 4,5-trisphosphate receptor isoforms expressed in COS-7 cells. J. Biol. Chem. *275*, 21492–21499.

Camacho, P., and Lechleiter, J.D. (1995). Calreticulin inhibits repetitive intracellular Ca^{2+} waves. Cell *82*, 765–771.

Caroppo, R., Colella, M., Colasuonno, A., DeLuisi, A., Debellis, L., Curci, S., and Hofer, A.M. (2003). A reassessment of the effects of luminal [Ca^{2+}] on inositol 1,4,5-trisphosphate-induced Ca^{2+} release from internal stores. J. Biol. Chem. *278*, 39503–39508.

Choe, C.U., Harrison, K.D., Grant, W., and Ehrlich, B.E. (2004). Functional coupling of chromogranin with inositol 1,4,5-trisphosphate receptor shapes calcium signaling. J. Biol. Chem. *279*, 35551–35556.

Foyouzi-Youssefi, R., Arnaudeau, S., Borner, C., Kelley, W.L., Tschopp, J., Lew, D.P., Demaurex, N., and Krause, K.H. (2000). Bcl-2 decreases the free Ca^{2+} concentration within the endoplasmic reticulum. Proc. Natl. Acad. Sci. USA *97*, 5723–5728.

Hattori, M., Suzuki, A.Z., Higo, T., Miyauchi, H., Michikawa, T., Nakamura, T., Inoue, T., and Mikoshiba, K. (2004). Distinct roles of inositol 1,4,5 trisphosphate receptor types 1 and 3. J. Biol. Chem. *279*, 11967–11975.

Hwang, C., Sinskey, A.J., and Lodish, H.F. (1992). Oxidized redox state of glutathione in the endoplasmic reticulum. Science *257*, 1496–1502.

Inoue, T., Kato, K., Kohda, K., and Mikoshiba, K. (1998). Type 1 inositol 1,4,5-trisphosphate receptor is required for induction of long-term depression in cerebellar Purkinje neurons. J. Neurosci. *18*, 5366–5373.

Kamp, F., Donoso, P., and Hidalgo, C. (1998). Changes in luminal pH caused by calcium release in sarcoplasmic reticulum vesicles. Biophys. J. *74*, 290–296.

Kim, J.H., Johannes, L., Goud, B., Antony, C., Lingwood, C.A., Daneman, R., and Grinstein, S. (1998). Noninvasive measurement of the pH of the endoplasmic reticulum at rest and during calcium release. Proc. Natl. Acad. Sci. USA *95*, 2997–3002.

Knapp, L.T., and Klann, E. (2002). Role of reactive oxygen species in hippocampal long-term potentiation: contributory or inhibitory? J. Neurosci. Res. *70*, 1–7.

Li, Y., and Camacho, P. (2004). Ca^{2+}-dependent redox modulation of SERCA 2b by ERp57. J. Cell Biol. *164*, 35–46.

Mattson, M.P. (2004). Pathways towards and away from Alzheimer's disease. Nature *430*, 631–639.

Meldolesi, J., and Pozzan, T. (1998). The endoplasmic reticulum Ca^{2+} store: a view from the lumen. Trends Biochem. Sci. *23*, 10–14.

Michikawa, T., Hirota, J., Kawano, S., Hiraoka, M., Yamada, M., Furuichi, T., and Mikoshiba, K. (1999). Calmodulin mediates calcium-dependent inactivation of the cerebellar type 1 inositol 1,4,5-trisphosphate receptor. Neuron *23*, 799–808.

Nishiyama, M., Hong, K., Mikoshiba, K., Poo, M.M., and Kato, K. (2000). Calcium stores regulate the polarity and input specificity of synaptic modification. Nature *408*, 584–588.

Orrenius, S., Zhivotovsky, B., and Nicotera, P. (2003). Regulation of cell death: the calcium-apoptosis link. Nat. Rev. Mol. Cell Biol. *4*, 552–565.

Paschen, W. (2003). Mechanisms of neuronal cell death: diverse roles of calcium in the various subcellular compartments. Cell Calcium *34*, 305–310.

Patterson, R.L., Boehning, D., and Snyder, S.H. (2004). Inositol 1,4,5-trisphosphate receptors as signal integrators. Annu. Rev. Biochem. *73*, 437–465.

Ro, H.A., and Carson, J.H. (2004). pH microdomains in oligodendrocytes. J. Biol. Chem. *279*, 37115–37123.

Roderick, L.H., Llewellyn, D.H., Campbell, A.K., and Kendall, J.M. (1998). Role of calreticulin in regulating intracellular Ca^{2+} storage and capacitative Ca^{2+} entry in HeLa cells. Cell Calcium *24*, 253–262.

Sevier, C.S., and Kaiser, C.A. (2002). Formation and transfer of disulphide bonds in living cells. Nat. Rev. Mol. Cell Biol. *3*, 836–847.

Stutzmann, G.E., Caccamo, A., LaFerla, F.M., and Parker, I. (2004). Dysregulated IP_3 signaling in cortical neurons of knock-in mice expressing an Alzheimer's-linked mutation in presenilin1 results in exaggerated Ca^{2+} signals and altered membrane excitability. J. Neurosci. *24*, 508–513.

Sugawara, H., Kurosaki, M., Takata, M., and Kurosaki, T. (1997). Genetic evidence for involvement of type 1, type 2 and type 3 inositol

1,4,5-trisphosphate receptors in signal transduction through the B-cell antigen receptor. EMBO J. *16*, 3078–3088.

Takei, K., Shin, R.M., Inoue, T., Kato, K., and Mikoshiba, K. (1998). Regulation of nerve growth mediated by inositol 1,4,5-trisphosphate receptors in growth cones. Science *282*, 1705–1708.

Tang, T.S., Tu, H., Chan, E.Y., Maximov, A., Wang, Z., Wellington, C.L., Hayden, M.R., and Bezprozvanny, I. (2003). Huntingtin and huntingtin-associated protein 1 influence neuronal calcium signaling mediated by inositol-(1,4,5) trisphosphate receptor type 1. Neuron *39*, 227–239.

Taylor, C.W., Genazzani, A.A., and Morris, S.A. (1999). Expression of inositol trisphosphate receptors. Cell Calcium *26*, 237–251.

Thrower, E.C., Choe, C.U., So, S.H., Jeon, S.H., Ehrlich, B.E., Yoo, S.H. (2003). A functional interaction between chromogranin B and the inositol 1,4,5-trisphosphate receptor/Ca^{2+} channel. J. Biol. Chem. *278*, 49699–49706.

Tu, B.P., and Weissman, J.S. (2002). The FAD- and O_2-dependent reaction cycle of Ero1-mediated oxidative protein folding in the endoplasmic reticulum. Mol. Cell *10*, 983–994.

Xiang, Y., Li, Y., Zhang, Z., Cui, K., Wang, S., Yuan, X.B., Wu, C.P., Poo, M.M., and Duan, S. (2002). Nerve growth cone guidance mediated by G protein-coupled receptors. Nat. Neurosci. *5*, 843–848.